

Evidence for a molecular rotational band in the $^{14}\text{C} + \alpha$ decay of ^{18}O and the α decay of ^{22}Ne

N. Curtis

*Department of Physics, Florida State University, Tallahassee, Florida 32306
and School of Physics and Astronomy, University of Birmingham, Edgbaston, Birmingham B15 2TT, United Kingdom*

D. D. Caussyn, C. Chandler,* M. W. Cooper, N. R. Fletcher, R. W. Laird,† and J. Pavan

Department of Physics, Florida State University, Tallahassee, Florida 32306

(Received 1 March 2002; published 16 August 2002)

The $^{14}\text{C} + \alpha$ decay of ^{18}O has been studied via the $^{14}\text{C}(^{18}\text{O}, ^{14}\text{C}\alpha)^{14}\text{C}$ reaction at 102 MeV. The excitation energy of the decaying ^{18}O resonant particle has been determined following the coincident detection of the correlated ^{14}C and α particles. A study of the angular correlations of the breakup fragments has allowed the spins of the decaying states to be investigated. The data provide evidence that a quasimolecular rotational band, identified by enhanced α decay, is observed in the reaction. Evidence is also presented for the $^{18}\text{O} + \alpha$ decay of ^{22}Ne .

DOI: 10.1103/PhysRevC.66.024315

PACS number(s): 23.60.+e, 27.20.+n, 27.30.+t

I. INTRODUCTION

The $^{14}\text{C} + \alpha$ cluster structure of ^{18}O is reasonably well established. Much work has been performed in studying both the rotational $^{14}\text{C} + \alpha$ quasimolecular nature of ^{18}O [up to $E_x(^{18}\text{O}) \sim 12.5$ MeV] and the nuclear-astrophysically important radiative capture reaction $^{14}\text{C}(\alpha, \gamma)^{18}\text{O}$ (see, for example, Refs. [1–7] and references contained therein). The α decay of a number of states at a high excitation energy, above the α -decay threshold at 6.226 MeV, has been studied in the past by Rae and Bhowmik [8] via the $^{12}\text{C}(^{18}\text{O}, ^{14}\text{C}\alpha)^{12}\text{C}$ sequential breakup reaction at 82 MeV. Spin information was obtained for some of the observed states following a study of the variation in double-differential cross section with the scattering angle of the $^{18}\text{O}^*$ nucleus. The majority of the assignments made by Rae and Bhowmik are tentative, however, with two possible spin and parities being listed for many states.

In an attempt to clarify the spin assignments of Rae and Bhowmik we have performed a measurement of the $^{14}\text{C}(^{18}\text{O}, ^{14}\text{C}\alpha)^{14}\text{C}$ breakup reaction at 102 MeV. This entrance channel was selected to allow a simultaneous search for α -particle decay of additional neutron rich nuclei. Coincident detection of the ^{14}C and α breakup fragments emitted during the decay of $^{18}\text{O}^*$ has allowed the excitation energy in $^{18}\text{O}^*$ and the fragment angular correlations to be studied. The data suggest that a quasimolecular rotational band, consistent with a $^{14}\text{C} + \alpha$ structure, is populated in the reaction. Evidence is also provided for the $^{18}\text{O} + \alpha$ decay of a number of highly excited states in ^{22}Ne .

II. EXPERIMENTAL DETAILS

The experiment made use of a 102-MeV ^{18}O beam provided by the Florida State University tandem and supercon-

ducting LINAC facility. The beam was not debunched following LINAC acceleration resulting in a beam energy spread of ~ 800 keV. The integrated beam exposure was 3.5 mC.

The beam was used to bombard a $413\text{-}\mu\text{g cm}^{-2}$ ^{14}C target that was mounted between two thin ($\sim 10 \mu\text{g cm}^{-2}$) layers of formvar to aid mechanical stability. The ^{14}C thickness was obtained by studying the elastic scattering of a 24-MeV ^{16}O beam from a ^{197}Au foil placed downstream from the primary target location with the ^{14}C target both in position and removed. The target was surrounded by a containment system as a precaution against chamber contamination. This consisted of a 10 cm diameter vertical aluminum cylinder placed on the floor of the target chamber and centered at the target position. A 6 mm hole provided the beam entrance aperture and the exit port was a horizontal slot, 9.5 mm high and $\pm 35^\circ$ wide, symmetrically located with respect to the beam. Permanent magnets were placed close to the target at the angular extremes of the exit slot to deflect β particles away from the horizontal reaction plane, preventing them from reaching the detectors. α particles from ^{241}Am were vertically deflected by less than $100 \mu\text{m}$ at the detector positions.

Two identical telescopes were used to detect the breakup fragments. Each consisted of two (50×10) mm² silicon detectors placed one behind the other with the longer axis placed horizontally in the reaction plane defined by the two telescopes and the target. The detectors were nominally 68 and 1000 μm thick, allowing standard ΔE - E particle identification to be obtained. Mass separation was obtained up to the beryllium isotopes with $^{7,9,10}\text{Be}$ being resolved. This suggests that it would have been possible to cleanly resolve the isotopes $^4,^6\text{He}$. No evidence for ^6He was found in the particle identification spectra. It follows that the reaction $^{18}\text{O}^* \rightarrow ^{12}\text{C} + ^6\text{He}$ was not contaminating the $^{18}\text{O}^* \rightarrow ^{14}\text{C} + \alpha$ reconstruction. The carbon isotopes $^{12,13,14}\text{C}$ were not completely resolved in the ΔE - E spectra. It is therefore possible that some contaminant events, most likely involving ^{13}C ,

*Present address: School of Chemistry and Physics, Keele University, Keele, Staffordshire ST5 5BG, United Kingdom.

†Present address: Department of Medical Physics, University of Wisconsin-Madison, Madison, WI 53706.

passed through the ^{14}C particle identification gate. These events may be distinguished and removed, however, following the Q -value considerations. Each detector provided in-plane position information with a resolution of ~ 0.5 mm. The average beam current was maintained at ~ 5 enA to keep the counting rate in the detector telescopes ≤ 6 kHz. Above this rate the position resolution is known to deteriorate. Out-of-plane position information was limited to the detector height. The telescopes were placed on opposite sides of the beam with centers located at 18.5° from the beam axis. This geometry was selected to allow the possible detection of symmetric breakup from a number of reaction channels. The target to E detector distance was set to 140 mm, giving an angular range of $\pm 10.1^\circ$ about the detector center.

In order to calibrate the position response of the detectors, brass masks were placed in front of each telescope, 120 mm from the target. Each mask had nine equally spaced vertical slots to provide a horizontal position calibration along the detector face. The energy calibrations were performed using a combination of α particles from a ^{228}Th source and from the $^{12}\text{C}(^{12}\text{C}, \alpha)^{20}\text{Ne}^*$ reaction at 25 and 45 MeV. Additional calibrations were obtained using ^{12}C ions elastically scattered from a ^{197}Au target at beam energies of 16, 20, 25, 40, 45, and 51 MeV. The energy resolution was found to be 50 keV for α particles from the decay of ^{228}Th and 120 keV for ^{12}C at 25 MeV.

III. ANALYSIS AND RESULTS

The method of resonant particle decay spectroscopy is an established technique used in the study of breakup reactions [9]. Once the two fragments have been identified using the information provided by the $(\Delta E-E)$ telescopes, the kinematics of the undetected recoil particle can be reconstructed and the three-body reaction Q value (Q_3) studied. The recoil energy is obtained by applying momentum conservation between the beam and the two detected particles and by making an assumption of the recoil mass. The summed energy of the three final-state particles is related to the Q value via $E_{\text{tot}} = E_1 + E_2 + E_{\text{rec}} = E_{\text{beam}} + Q_3$.

Following channel identification the excitation energy (E_x) of the resonant particle may be determined by studying the relative energy (E_{rel}) of the two breakup fragments, $E_x = E_{\text{rel}} - Q_2$, where Q_2 is the Q value for the decay into fragments 1 and 2. Spin information for states observed in the E_x spectrum may be obtained from a study of the breakup fragment angular correlations (see, for example, Refs. [10,11]). The two angles involved are θ^* , the center-of-mass (c.m.) scattering angle of the resonant particle, and ψ , the angle between the relative velocity vector of the two breakup fragments and the beam axis. A plot of θ^* versus ψ will exhibit intensity variations that form ‘‘ridges’’ in the data. The ψ distribution at $\theta^* = 0^\circ$, obtained by projecting the data along the slope of the ridges, is denoted ψ_0 . This may be compared to squared Legendre polynomials $|P_J|^2$, the spin of the decaying state being equal to the order J of the polynomial best describing the ψ_0 distribution.

The slope of the ridges along which the angular correlations are projected, $d\theta^*/d\psi$, and the order of the overlaid

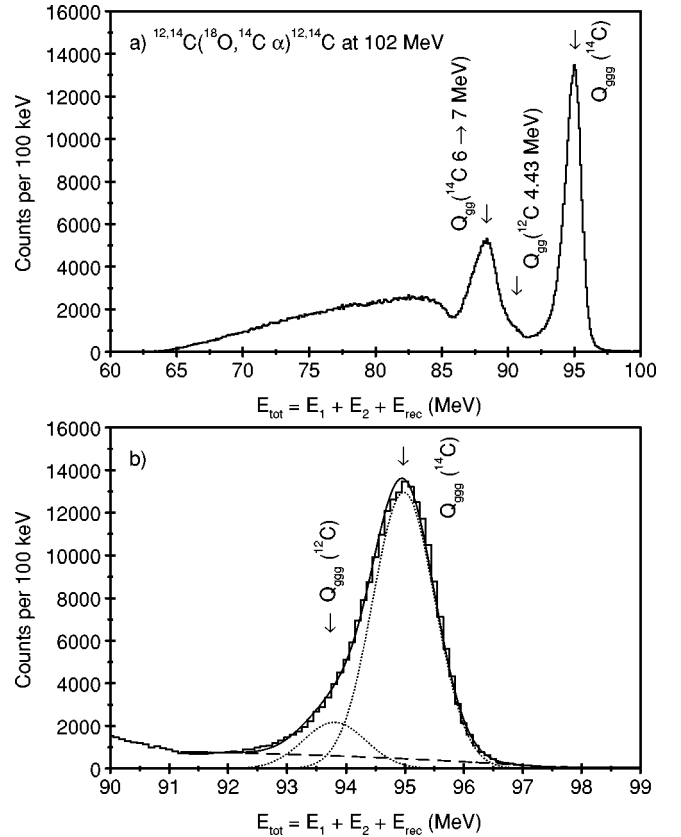


FIG. 1. Total energy (E_{tot}) spectrum for the $^{12,14}\text{C}(^{18}\text{O}, ^{14}\text{C} \alpha)^{12,14}\text{C}$ reaction. The recoil mass has been assumed to be 14. In (a) the predicted E_{tot} values for the $^{14}\text{C}(^{18}\text{O}, ^{14}\text{C}_{\text{g.s.}} \alpha)^{14}\text{C}_{\text{g.s.}}$, $^{12}\text{C}(^{18}\text{O}, ^{14}\text{C}_{\text{g.s.}} \alpha)^{12}\text{C}^*(4.43 \text{ MeV})$, and $^{14}\text{C}(^{18}\text{O}, ^{14}\text{C}_{\text{g.s.}} \alpha)^{14}\text{C}^*(6 \rightarrow 7 \text{ MeV})$ reactions are shown. In (b) an expanded Q_{ggg} region is shown to indicate the ^{12}C contribution. The results of a two Gaussian plus background fit are indicated by the smooth solid line, the background by the dashed line, and the individual fitted peaks by the two dotted lines.

Legendre polynomial may be used [11] to determine the entrance channel grazing angular momentum l_i by using

$$\frac{d\theta^*}{d\psi} = \frac{J}{l_i - J}. \quad (1)$$

Conversely, assuming l_i is known Eq. (1) can provide an independent spin assignment to that obtained from the angular correlation projection method described above.

A. The α decay of ^{18}O

The total energy (E_{tot}) spectrum obtained following the detection of an α particle and ^{14}C in the detector telescopes is shown in Fig. 1. In this analysis the recoil has been assumed to be ^{14}C . In Fig. 1(a) the predicted E_{tot} energy for events corresponding to the $^{14}\text{C}(^{18}\text{O}, ^{14}\text{C}_{\text{g.s.}} \alpha)^{14}\text{C}_{\text{g.s.}}$ reaction is labeled as $Q_{\text{ggg}}(^{14}\text{C})$. A strong peak is observed at this energy. This peak may also contain events from the $^{12}\text{C}(^{18}\text{O}, ^{14}\text{C}_{\text{g.s.}} \alpha)^{12}\text{C}_{\text{g.s.}}$ channel arising from the ^{12}C content of the formvar and the ^{14}C target. This reaction has the same value of Q_3 , although the use of the incorrect recoil mass in

the reconstruction will result in a shifting of the Q_{ggg} peak towards lower values of E_{tot} for these events. Evidence for reactions from ^{12}C may indeed be seen in Fig. 1(a) as a shoulder at 90.6 MeV [labeled $Q_{ggg}(^{12}\text{C} \ 4.43 \ \text{MeV})$], these events corresponding to the $^{12}\text{C}(^{18}\text{O}, ^{14}\text{C}_{g.s.}, \alpha)^{12}\text{C}^*(4.43 \ \text{MeV})$ reaction. The peak appearing at $E_{tot} \sim 88.3 \ \text{MeV}$, labeled $Q_{ggg}(^{14}\text{C} 6 \rightarrow 7 \ \text{MeV})$ corresponds to a mixture of the $^{14}\text{C}(^{18}\text{O}, ^{14}\text{C} \ \alpha)^{14}\text{C}$ reaction with one of the two ^{14}C nuclei emitted in an excited state (the first excited state in ^{14}C is at 6.09 MeV) and the $^{12}\text{C}(^{18}\text{O}, ^{14}\text{C} \ \alpha)^{12}\text{C}$ channel with the ^{12}C recoil excited to the second excited state (or higher). Possible contaminant reactions arising from misidentification of the detected particles include

$$^{12}\text{C}(^{18}\text{O}, ^{13}\text{C} \ \alpha)^{13}\text{C} \ (Q_3 = -9.46 \ \text{MeV}),$$

$$^{14}\text{C}(^{18}\text{O}, ^{13}\text{C} \ \alpha)^{15}\text{C} \ (Q_3 = -13.18 \ \text{MeV}),$$

$$^{14}\text{C}(^{18}\text{O}, ^{12}\text{C} \ \alpha)^{16}\text{C} \ (Q_3 = -13.88 \ \text{MeV}),$$

$$^{12}\text{C}(^{18}\text{O}, ^{12}\text{C} \ ^6\text{He})^{12}\text{C} \ (Q_3 = -18.37 \ \text{MeV}),$$

and $^{14}\text{C}(^{18}\text{O}, ^{12}\text{C} \ ^6\text{He})^{14}\text{C} \ (Q_3 = -18.37 \ \text{MeV})$.

All of these channels have values of Q_3 that are much more negative than the $^{14}\text{C}(^{18}\text{O}, ^{14}\text{C}_{g.s.}, \alpha)^{14}\text{C}_{g.s.}$ reaction of interest ($Q_3 = -6.23 \ \text{MeV}$) and will therefore appear at lower values of E_{tot} than the $Q_{ggg}(^{14}\text{C})$ peak.

In Fig. 1(b) the E_{tot} spectrum is shown with an expanded scale. The Q_{ggg} peak has been fitted with two Gaussians (dotted lines) and a smooth background (dashed line). The overall fit is given by the smooth solid line. The Gaussians correspond to the $^{14}\text{C}(^{18}\text{O}, ^{14}\text{C}_{g.s.}, \alpha)^{14}\text{C}_{g.s.}$ and $^{12}\text{C}(^{18}\text{O}, ^{14}\text{C}_{g.s.}, \alpha)^{12}\text{C}_{g.s.}$ channels. A Monte Carlo simulation of the experimental resolution predicts widths of 1250 keV for the $Q_{ggg}(^{14}\text{C})$ peak and 1310 keV for the $Q_{ggg}(^{12}\text{C})$ peak with a uncertainty of approximately 50 keV. The Monte Carlo code [12] simulates various effects including the energy loss and energy and angular straggling of the beam and fragments in the target and the energy and position resolution of the detector telescopes. The fitted widths of the $Q_{ggg}(^{12}\text{C})$ and $Q_{ggg}(^{14}\text{C})$ peaks shown in Fig. 1(b) are approximately 1230 keV, in good agreement with the predicted values. The ratio of ^{12}C to ^{14}C , $R(^{12}\text{C}:^{14}\text{C})$, in the combined formvar and ^{14}C target can be obtained from the number of events (N) above background in the two peaks. This gives a relative carbon content of $\sim 85\%$ ^{14}C and $\sim 15\%$ ^{12}C . These values have been scaled by the ratio of the target masses to approximate the difference in reaction cross sections from the two target nuclei, $R(^{12}\text{C}:^{14}\text{C}) = N[Q_{ggg}(^{12}\text{C})]/12: N[Q_{ggg}(^{14}\text{C})]/14$.

In order to cleanly select events from the $^{14}\text{C}(^{18}\text{O}, ^{14}\text{C}_{g.s.}, \alpha)^{14}\text{C}_{g.s.}$ reaction, a spectrum is produced of $E_{rec} - Q_3 = E_{beam} - E_1 - E_2$ plotted against $P_{rec}^2/2$, where P_{rec} is the recoil momentum. This is shown in Fig. 2. In this spectrum the Q_{ggg} events from the ^{14}C content of the target will lie on a line with a slope of $1/m_{rec} = 1/14$, whereas events from the ^{12}C will have a slope of $1/12$. Both loci will have an intercept on the $E_{rec} - Q_3$ axis equal to Q_3 ,

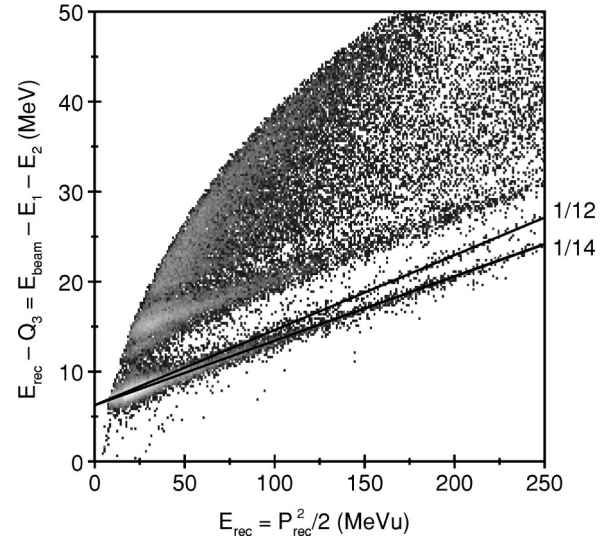


FIG. 2. Plot of $(E_{rec} - Q_3)$ against $P_{rec}^2/2$ for the $^{12,14}\text{C}(^{18}\text{O}, ^{14}\text{C} \ \alpha)^{12,14}\text{C}$ reaction. The predicted Q_{ggg} loci with slopes of $1/12$ and $1/14$ (1/recoil mass) and the intercept at $-Q_3 = 6.23 \ \text{MeV}$ are indicated by the solid lines.

$-6.23 \ \text{MeV}$. Placing a software window around the events with a slope of $1/14$ allows the $^{14}\text{C}(^{18}\text{O}, ^{14}\text{C}_{g.s.}, \alpha)^{14}\text{C}_{g.s.}$ channel to be selected.

It is possible to reconstruct $E_{rel}(^{14}\text{C} + \alpha)$ in two ways in this channel. In Fig. 3 the E_x spectrum for ^{18}O obtained from the detected ^{14}C fragment, $^{14}\text{C}_{detected} + \alpha$, is plotted against the excitation energy calculated using the reconstructed recoil, $^{14}\text{C}_{recoil} + \alpha$. Strongly populated states are seen as vertical loci at ~ 8 and $11.6 \ \text{MeV}$ in the $^{14}\text{C}_{detected} + \alpha$ breakup. The $11.6 \ \text{MeV}$ state is also seen as a horizontal line in the $^{14}\text{C}_{recoil} + \alpha$ channel. There is no evidence in Fig. 3 for diagonal loci corresponding to the $^{14}\text{C} + ^{14}\text{C}$ decay of ^{28}Mg .

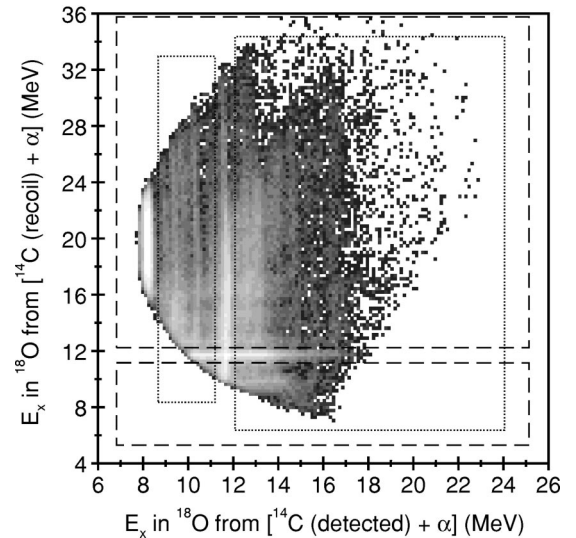


FIG. 3. Excitation energy for the $^{14}\text{C} + \alpha$ breakup of ^{18}O obtained with the detected ^{14}C plotted against the excitation energy calculated using the undetected (reconstructed) recoiling ^{14}C . The dotted and dashed boxes indicate the regions used to gate out the strong doublet at $\sim 8 \ \text{MeV}$ and the state at $11.6 \ \text{MeV}$.

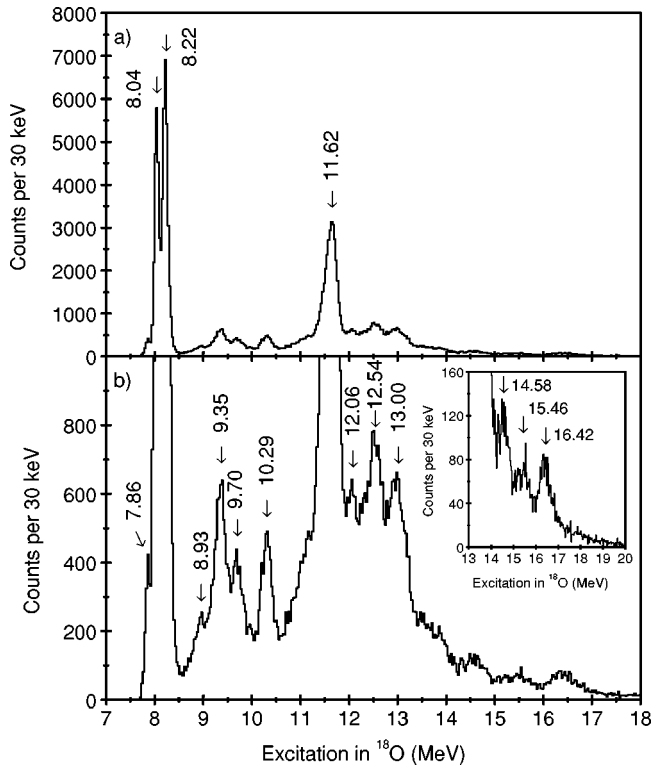


FIG. 4. Excitation energy spectrum for the $^{14}\text{C} + \alpha$ breakup of ^{18}O obtained using the detected ^{14}C fragment. The data are projected from within the two dashed boxes indicated in Fig. 3. In (b) the scaling has been altered to allow the less populated states to appear more prominently. In the inset to (b) the higher excitation region is shown. The fitted centroid energies of the peaks are given.

In Fig. 4 the excitation energy spectrum for the $^{14}\text{C}_{\text{detected}} + \alpha$ breakup of ^{18}O is shown. Only those events falling within the two dashed boxes indicated in Fig. 3 have been included. This gating removes background from the strongly populated ~ 11.6 MeV state seen in the $^{14}\text{C}_{\text{recoil}} + \alpha$ channel. In Fig. 4(a) the whole spectrum is shown. In Fig. 4(b) the same spectrum is shown with an expanded scale to allow the less strongly populated states to be seen. The inset in Fig. 4(b) shows the high- E_x region in more detail. The centroid energies of the states, obtained by fitting Gaussian line shapes to the peaks above a smoothly varying background, are indicated and given in Table I. Also listed are the energies and spin assignments given in the compilation for ^{18}O by Tilley *et al.* [13]. It is possible, by comparing the states observed in the excitation energy spectra shown in Fig. 4 and in Ref. [8], to make a direct association between the present and previous measurements and to those listed in Ref. [13]. The final excitation energy calibration for the present work was obtained by this method. It is noted that in the compilation for ^{18}O Tilley *et al.* [13] list 50 known states in the excitation energy range 8.0–13.0 MeV, 31 of which decay via α emission. Only ten states are seen in this energy interval in Fig. 4. This suggests that there may be a structural reason for the preferential α decay of the observed states. It is possible that the enhanced relative strength is due to an underlying $^{14}\text{C} + \alpha$ cluster structure. This would be analogous to the well-known $^{12}\text{C} + ^{12}\text{C}$ breakup of the hyperde-

TABLE I. States observed in $^{18}\text{O}^* \rightarrow ^{14}\text{C} + \alpha$ and corresponding states from Ref. [13].

Present work		Tilley <i>et al.</i> [13]			
E_x (MeV)	J^π (\hbar)	l_i (\hbar)	E_x (MeV)	J^π (\hbar)	$\Gamma_{\text{c.m.}}$ (keV)
7.86			7.864	5^-	
8.04 ^a			8.038	1^-	$< 2.5^b$
8.22 ^{a(c)}			8.213	2^+	1.0 ± 0.8^b
8.93			8.955	(4^+)	43 ± 3^b
9.35 ^a	(2^+)	33 ± 2	9.361	2^+	27 ± 15^b
	(3^-)	31 ± 1			
9.70 ^{a,c}	(1^-)	26 ± 2	9.672	3^-	$< 50^b$
	(2^+)	34 ± 2			
	(3^-)	33 ± 1			
10.29 ^{a(c)}	(3^-)	29 ± 1	10.295	4^+	$< 50^b$
	(4^+)	28 ± 1			
	(5^-)	25 ± 1			
11.62 ^{a,c}	5^-	31 ± 1	11.620	5^-	$(76 \pm 8)^d$
12.06			12.04	(2^+)	28 ± 6^b
12.54 ^{a,c}			12.530	6^+	$< 250^e$
13.00	(2^+)	25 ± 2			$< 300^e$
	(4^+)	28 ± 2			
14.58 ^c			14.7	1^-	$\sim 500^e$
15.46					$\sim 500^e$
16.42 ^(c)			16.315	$(3,2)^-$	$\sim 600^e$

^aMembers of the molecular band in ^{18}O .

^bReference [13].

^cStates that are also observed in $^{18}\text{O}^* \rightarrow ^{14}\text{C}_{\text{recoil}} + \alpha$.

^dReference [16].

^ePresent work.

formed quasimolecular rotational band in ^{24}Mg (see, for example, Ref. [14]). This occurs in the excitation energy range 20–30 MeV, a region in which a level density of above 1000 states per MeV would be expected. The $^{12}\text{C} + ^{12}\text{C}$ decay, observed in the $^{12}\text{C}(^{24}\text{Mg}, ^{12}\text{C}^{12}\text{C})^{12}\text{C}$ reaction, is actually observed only from approximately ten states. This has been interpreted as being due to an underlying $^{12}\text{C} + ^{12}\text{C}$ cluster structure that has a large overlap with the ^{24}Mg ground-state configuration.

The excitation energy spectrum obtained from the $^{14}\text{C}_{\text{recoil}} + \alpha$ channel is plotted in Fig. 5. Only events falling within the two dotted regions indicated in Fig. 3 are included. This removes the large background from the 8.04, 8.22, and 11.62 MeV states observed in the $^{14}\text{C}_{\text{detected}} + \alpha$ breakup. In Fig. 5(a) the whole spectrum is shown and in Fig. 5(b) the data are plotted on an expanded scale to allow the weaker states to be seen. As for the $^{14}\text{C}_{\text{detected}} + \alpha$ excitation energy spectrum shown in Fig. 4 the energy scale has again been calibrated to the work of Refs. [8,13], although only the 9.7 and 11.6 MeV states could be used in the comparison with Rae and Bhowmik [8]. A number of states are observed in the $^{14}\text{C}_{\text{recoil}} + \alpha$ channel, the centroid energies being noted in Fig. 5. The agreement between these states and those seen in Fig. 4 is generally good up to and including the state at 12.6 MeV. At higher excitations the experimental

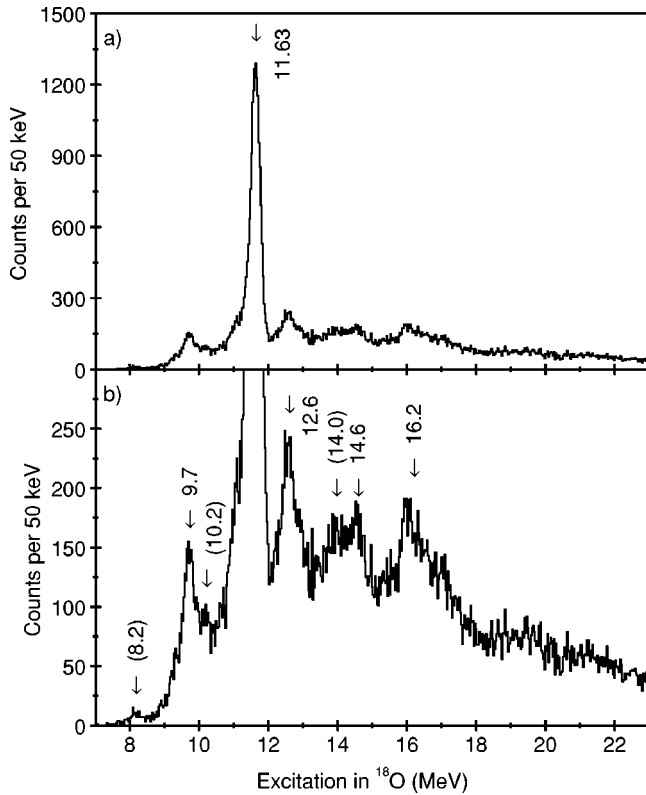


FIG. 5. Excitation energy spectrum for the $^{14}\text{C} + \alpha$ breakup of ^{18}O obtained using the undetected ^{14}C recoil. The data are projected from within the two dotted boxes indicated in Fig. 3.

resolution in the $^{14}\text{C}_{\text{recoil}} + \alpha$ channel degrades making a direct comparison more difficult. This is due to the much lower energy of the detected ^{14}C , which, in this channel, is the recoiling particle. The lower energy results in greater energy loss and energy and angular straggling in the target. It is noted that the strongly populated state at 10.29 MeV in Fig. 4 appears to be very weakly populated in Fig. 5. This is most likely due to the difference in the c.m. angular coverage for the detected and recoiling ^{14}C nuclei. This may also hold true for the 12.06 and 13.0 MeV states that do not appear in the $^{14}\text{C}_{\text{recoil}} + \alpha$ channel, although the three states seen at 12.06, 12.54, and 13.0 MeV in Fig. 4 may well be unresolved as the broad (500 keV wide) peak at 12.6 MeV in Fig. 5. The structure at ~ 14.6 MeV in the $^{14}\text{C}_{\text{recoil}} + \alpha$ channel most likely corresponds to the peak at 14.58 MeV in the $^{14}\text{C}_{\text{detected}} + \alpha$ breakup. The broad ~ 16.2 MeV peak in Fig. 5 probably corresponds to the 16.42 MeV state in Fig. 4.

Tentative spin assignments have been obtained for some of the states observed in Fig. 4 from a study of the breakup fragment angular correlations. A plot of θ^* versus ψ for the strong state seen at 11.62 MeV in Fig. 4 is shown in Fig. 6. The two regions of data seen in the θ^*/ψ angular correlation correspond to the two possible ways of detecting the breakup, $^{14}\text{C} + \alpha$ and $\alpha + ^{14}\text{C}$, in the two telescopes. Within each of the two regions clear ridges may be seen in the data, the slope of which is indicated by the dashed line. The loci of events with negative slope, indicated by the dotted lines in Fig. 6, correspond to background from the $^{14}\text{C}_{\text{recoil}} + \alpha$ chan-

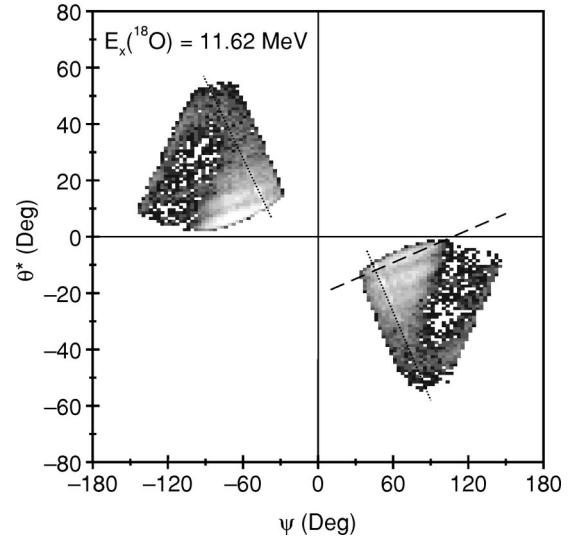


FIG. 6. Angular correlation (θ^*/ψ) spectrum for the 11.62-MeV state seen in Fig. 4. The dashed and dotted lines are discussed in the text.

nel. These have been removed using software gates before projecting the data onto the $\theta^* = 0^\circ$ axis.

In Figs. 7 and 8 the projected angular correlations obtained are shown. Some states listed in Table I do not have projections, either as a result of poor statistics or limited θ^*/ψ coverage. It is unfortunate that the two most strongly populated states, at 8.04 and 8.22 MeV, fall in the second category, although firm assignments of 1^- and 2^+ , respectively, were made previously by Rae and Bhowmik [8]. Several of the states are shown at more than one projection angle, each overlaid with a different order of $|P_J|^2$. For example, the 9.35-MeV-state data may be described by a $|P_2|^2$ if projected at 3.7° but equally as well by a $|P_3|^2$ if projected at 6.1° . It is noted that it is the periodicity of the distribution that is important, not the magnitude. The inclusion of data projected from $\theta^* \neq 0^\circ$ will distort the magnitude of the theoretical $|P_J|^2$ correlation. This arises from the introduction of nonzero m -substates populations for $\theta^* \neq 0^\circ$ [11]. In addition, the experimental data have not been corrected for detection efficiency, which strongly distorts the $|P_J|^2$ distribution. Table I summarizes the tentative spin and parity assignments made for the states in the present work. It is noted that breakup may be seen only from natural parity states when both fragments have $J^\pi = 0^+$, as is the case here. In general, the agreement between the present work and Refs. [8,13] is good. The present assignment of $(2^+, 3^-)$ for the state at 9.35 MeV in Fig. 4 is the same as that made in Ref. [8], the firm assignment being listed as 2^+ in Ref. [13]. Similarly the spin of the 9.70 MeV state, tentatively $(1^-, 2^+, 3^-)$ in the present work, may be assigned as 3^- by comparison with Refs. [8,13] and that of the 10.29 MeV state as 4^+ .

The values of l_i obtained using Eq. (1) are listed in Table I. The range of experimental l_i values, $(25 \pm 1) - (34 \pm 2)\hbar$, agrees reasonably well with that calculated for two nuclei in the entrance channel with masses A_p and A_t , $l_i = r_0(A_p^{1/3} + A_t^{1/3})\sqrt{2\mu E_{\text{c.m.}}}$, where μ is the reduced mass and $E_{\text{c.m.}}$ the

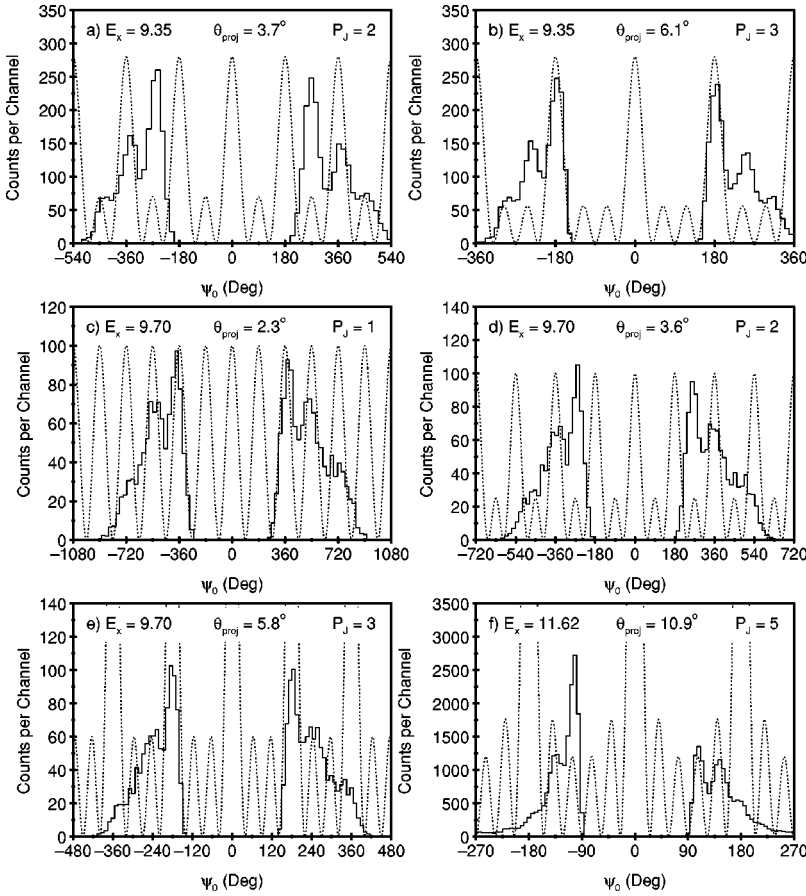


FIG. 7. Projections onto the $\theta^*=0^\circ$ axis for the θ^*/ψ angular correlations for the states at (a) and (b) 9.35, (c), (d), and (e) 9.70, and (f) 11.62 MeV excitation energy in ^{18}O . The projection angle used is indicated in all cases, as is the order J of the $|P_J|^2$ shown by the dotted lines.

energy of the c.m. system. For values of r_0 ranging from 1.3 to 1.5 fm l_i is found to vary from 26.8 to 30.9 \hbar .

In Fig. 9 the values of $J(J+1)$ for the most prominent states in Fig. 4 are plotted against the centroid energies (solid points). The spin assignments are those obtained by comparison with the previous work of Rae and Bhowmik [8] and Tilley *et al.* [13]. It can be seen that these states appear to lie on a trajectory indicative of a rotational band, which may be described using $E_x = E_0 + (\hbar^2/2I)J(J+1)$. Here E_0 is the bandhead energy and I the moment of inertia. The solid line in Fig. 9 indicates the results of such a fit to the states, from which values of $\hbar^2/2I = (110.4 \pm 1.4)$ keV and $E_0 = (8.10 \pm 0.03)$ MeV are obtained. This rotational parameter indicates that a structure with a high moment of inertia, and hence a large deformation, is populated in the reaction. The value of $\hbar^2/2I$ can be obtained in a semiclassical cluster configuration of $\alpha + {}^{14}\text{C}_{\text{g.s.}}$ with $r_0 = 1.5$ fm, but it requires the α and ${}^{14}\text{C}$ surface separation to be 2 fm. Such a large deformation of the molecular band states could be reduced if it could be shown that the ${}^{14}\text{C}$ is in an excited configuration, however, the data of Fig. 9 and Table I still provide a good indication that a highly deformed molecular structure is observed in ^{18}O in the ${}^{14}\text{C}({}^{18}\text{O}, {}^{14}\text{C}_{\text{g.s.}}, \alpha){}^{14}\text{C}_{\text{g.s.}}$ reaction.

It is interesting to note that the proposed rotational band displayed in Fig. 9 shows only a slight odd/even parity splitting. The dashed line in Fig. 9 illustrates the effect, with the 8.22 MeV 2^+ state chosen rather than the 9.35 MeV 2^+ state due to its much stronger α decay (see Fig. 4). The odd/even band splitting has been observed to be much more pro-

nounced in some neighboring nuclei of similar mass. The values of $\hbar^2/2I$ for $K^\pi = 0^+$ bands are approximately 209 keV for ${}^{16}\text{O}$ [15], 192 keV for ${}^{18}\text{O}$ [7], and 209 keV for ${}^{20}\text{Ne}$ [15]. All of these previously known bands require a core cluster to α cluster separation of approximately 2 fm less than the band in Fig. 9, which has $\hbar^2/2I = 110$ keV. It is precisely this increased cluster separation that nearly destroys the parity splitting, since it greatly increases the effect of the potential barrier between the cluster wells, thus producing a nearly pure $Y_{3,0}+$ quadrupole rotational band. Theoretical calculations, reviewed in Ref. [15], provide a reasonably good description of these neighboring bands by using $4p$ excitations of the ground states into the sd shell, however, higher configurations would be required to describe a band with much greater cluster separations.

The proposed band shown in Fig. 9 is suggested to be a $K=0$ band with the unobserved $J^\pi = 0^+$ member near $E_x \sim 7.0$ –7.5 MeV. This excitation energy is below the α -decay detection threshold of the current detector geometry (see Fig. 4). The energy threshold for α -particle emission from ${}^{18}\text{O}$ is at 6.228 MeV, suggesting that the proposed band head is too high in energy to be of astrophysical importance.

The integrated double differential cross section for the ${}^{14}\text{C}({}^{18}\text{O}, {}^{14}\text{C}_{\text{g.s.}}, \alpha){}^{14}\text{C}_{\text{g.s.}}$ reaction, with respect to the solid angles covered by the two telescopes, is $d^2\sigma/d\Omega_1 d\Omega_2 = (7.4 \pm 1.0)$ mb sr $^{-2}$.

B. The α decay of ${}^{22}\text{Ne}$

The total energy spectrum produced following the detection of a ${}^{10}\text{Be}$ and an α particle is shown in Fig. 10. The

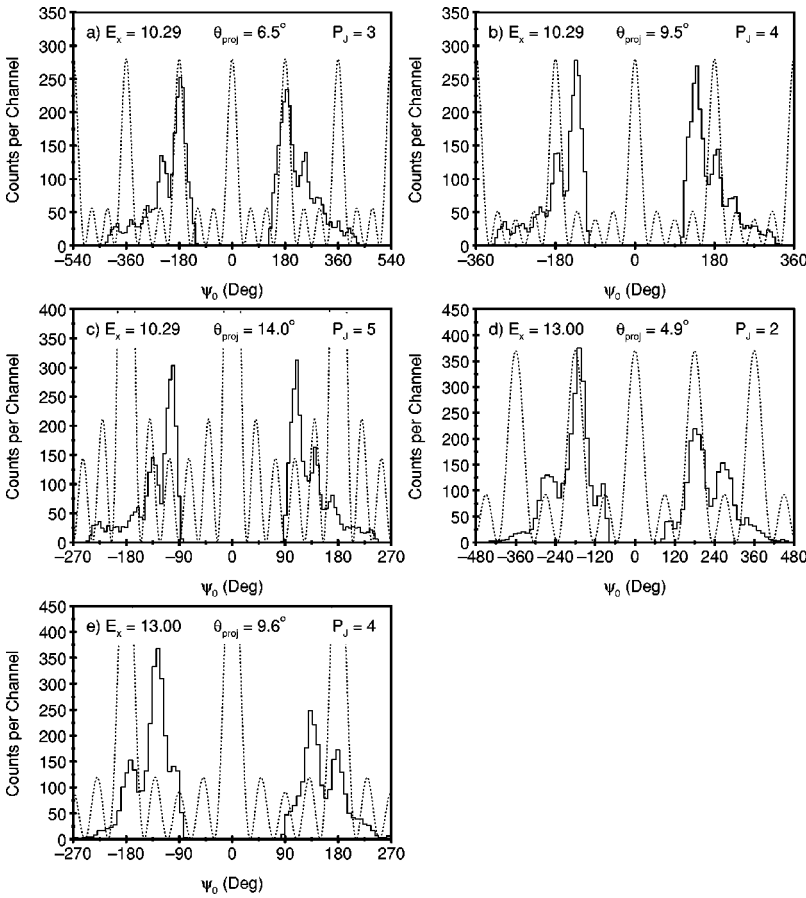


FIG. 8. Projections onto the $\theta^*=0^\circ$ axis for the θ^*/ψ angular correlations for the states at (a), (b), and (c) 10.29- and (d) and (e) 13.0-MeV excitation energy in ^{18}O . The projection angle used is indicated in all cases, as is the order J of the $|P_J|^2$ shown by the dotted lines.

predicted E_{tot} energy for the $^{14}\text{C}(^{18}\text{O}, ^{14}\text{C}^* \rightarrow ^{10}\text{Be}_{\text{g.s.}} + \alpha)^{18}\text{O}_{\text{g.s.}}$ and $^{14}\text{C}(^{18}\text{O}, ^{22}\text{Ne}^* \rightarrow ^{18}\text{O}_{\text{g.s.}} + \alpha)^{10}\text{Be}_{\text{g.s.}}$ reactions is labeled Q_{ggg} . Various other decay channels that involve excited final-state particles are also indicated. Events in the

peak labeled Q_{gg} (^{10}Be 3.37/ ^{18}O ~ 3.6 MeV) correspond to either a breakup involving a ^{10}Be emitted in the 3.37-MeV excited state or events with an ^{18}O excited to the 3.55-MeV 4^+ or 3.63-MeV 0^+ states. The Q -value resolution is not sufficient to resolve these channels. There is also a relatively strong peak at the predicted energy for the mutually excited

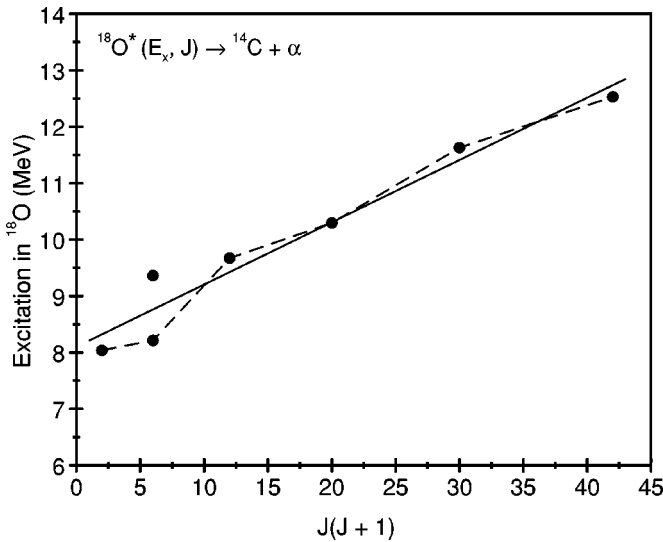


FIG. 9. Energy and spin systematics for the more prominent states observed the $^{14}\text{C} + \alpha$ decay of ^{18}O (solid points). The spin assignments from Ref. [13] are consistent with the current work. The solid line indicates a fit to the data and the dashed line is to guide the eye (see text).

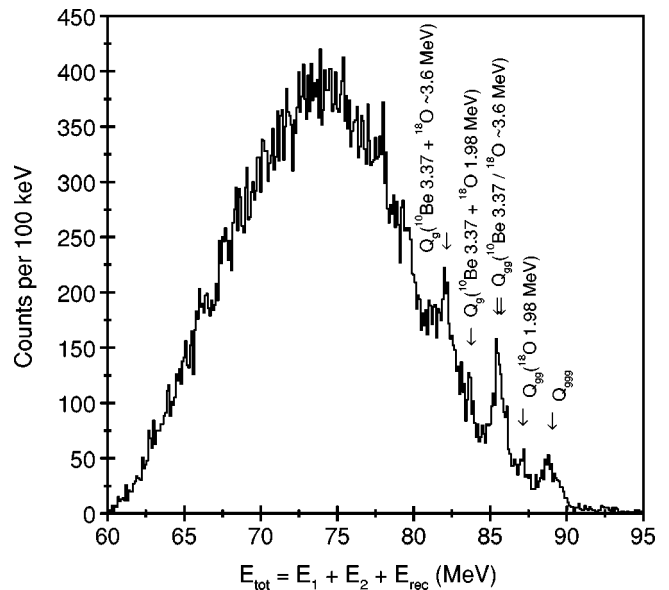


FIG. 10. Total energy (E_{tot}) spectrum for the $^{14}\text{C}(^{18}\text{O}, ^{18}\text{O}\alpha)^{10}\text{Be}$ reaction.

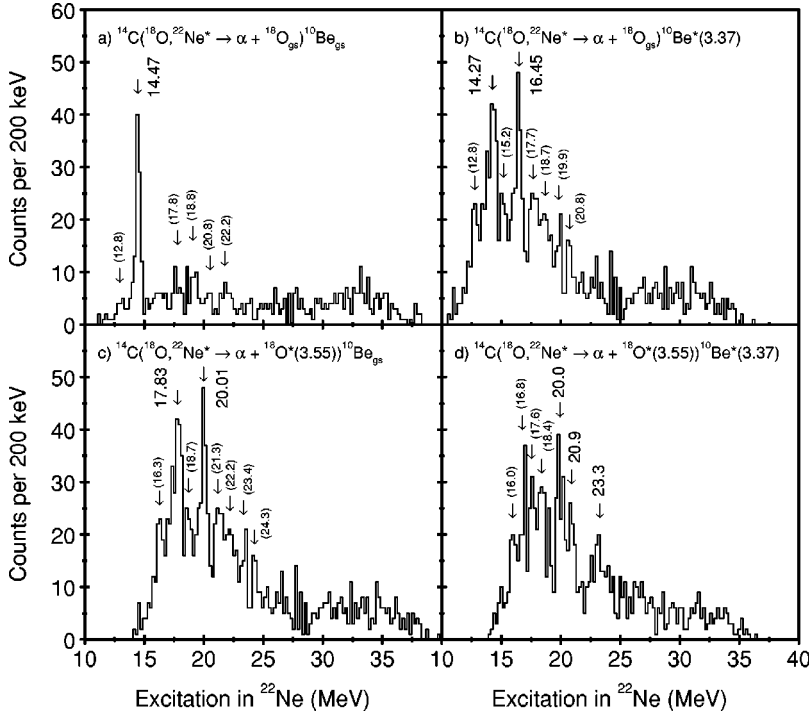


FIG. 11. Excitation energy spectra for the $^{18}\text{O} + \alpha$ breakup of ^{22}Ne using the reconstructed ^{18}O fragment and for different excitations of ^{18}O and ^{10}Be in the final state. The identical spectra in (b) and (c) have the same nominal value of Q_{gg} but have different values of E_x because of the assumed excitation in ^{18}O (see text).

$^{10}\text{Be}^*(3.37 \text{ MeV})$ and $^{18}\text{O}^*(\sim 3.6 \text{ MeV})$ reaction. This appears to sit on a shoulder corresponding to the $^{10}\text{Be}^* + \alpha + ^{18}\text{O}_{g.s.}$ final state, with the ^{10}Be being excited to one of the quartet of states near 6 MeV (5.958, 5.960, 6.179, and 6.263 MeV).

The excitation energy spectra for the $^{10}\text{Be} + \alpha$ decay of ^{14}C have been studied by gating on the Q_{ggg} , $Q_{gg}(^{10}\text{Be } 3.37/^{18}\text{O} \sim 3.6 \text{ MeV})$ and $Q_g(^{10}\text{Be } 3.37 + ^{18}\text{O} \sim 3.6 \text{ MeV})$ peaks shown in Fig. 10. The excitation energy spectra produced are featureless, indicating that α -particle decaying excited states of ^{14}C are not strongly populated in this reaction. The lack of structure in E_x suggests that the ^{10}Be and α particles arise from either direct (nonsequential) three body breakup or from the $^{18}\text{O} + \alpha$ decay of ^{22}Ne , with the detected ^{10}Be being the recoiling particle in the $^{14}\text{C}(^{18}\text{O}, ^{22}\text{Ne}^* \rightarrow ^{18}\text{O} + \alpha)^{10}\text{Be}$ reaction.

The $^{18}\text{O} + \alpha$ breakup of ^{22}Ne has been studied by producing excitation energy spectra using the reconstructed ^{18}O and the detected α particle. These are shown in Fig. 11. In Fig. 11(a) the E_x spectrum for ^{22}Ne is shown for those events falling within the Q_{ggg} peak in Fig. 10. One distinct state may be seen at 14.47 MeV (Table II). A spectrum such as that shown in Fig. 3 with E_x for ^{22}Ne obtained from the reconstructed ^{18}O plotted against the excitation energy calculated for ^{14}C using the detected ^{10}Be indicates that these events do indeed arise from the decay of ^{22}Ne . The integrated double-differential cross section for the $^{14}\text{C}(^{18}\text{O}, ^{22}\text{Ne}^* \rightarrow ^{18}\text{O}_{g.s.} + \alpha)^{10}\text{Be}_{g.s.}$ reaction is $d^2\sigma/d\Omega_1 d\Omega_2 = (0.025 \pm 0.003) \text{ mb sr}^{-2}$.

In Figs. 11(b) and 11(c) the data have been gated on the $Q_{gg}(^{10}\text{Be } 3.37/^{18}\text{O} \sim 3.6 \text{ MeV})$ peak observed in the total energy spectrum. If these events correspond mainly to the $^{14}\text{C}(^{18}\text{O}, ^{22}\text{Ne}^* \rightarrow ^{18}\text{O}_{g.s.} + \alpha)^{10}\text{Be}^*(3.37 \text{ MeV})$ reaction [as is assumed in Fig. 11(b)] then the excitation energy in ^{22}Ne

may be obtained from $E_{\text{rel}}(^{18}\text{O} + \alpha) - Q_2$. The sequential decay of the $^{22}\text{Ne}^*$ is not affected by the excitation energy carried by the recoiling ^{10}Be nucleus as this is produced in the initial $^{14}\text{C}(^{18}\text{O}, ^{22}\text{Ne}^*)^{10}\text{Be}^*$ reaction. However, if the $^{14}\text{C}(^{18}\text{O}, ^{22}\text{Ne}^* \rightarrow ^{18}\text{O}^*(\sim 3.6 \text{ MeV}) + \alpha)^{10}\text{Be}_{g.s.}$ channel dominates the events in the $Q_{gg}(^{10}\text{Be } 3.37/^{18}\text{O} \sim 3.6 \text{ MeV})$ peak then the excitation energy carried by ^{18}O must be taken into account. In this case $E_x(^{22}\text{Ne}) = E_{\text{rel}}(^{18}\text{O} + \alpha) - Q_2 + E_x(^{18}\text{O}^*)$. Hence the excitation energy spectrum shown in Fig. 11(c) differs from that in Fig. 11(b) only by a shift in energy scale. This has been taken to be +3.55 MeV. The integrated double-differential cross section for the events

TABLE II. Excitation energies in ^{22}Ne observed in α decay. The centroids listed in columns (a)–(d) are taken from the corresponding sections of Fig. 11. Excitations corroborated in two or more channels, except for the strong decay to the ground states for $E_x(^{22}\text{Ne}) = 14.47 \text{ MeV}$, are listed in the final column.

Centroids from Fig. 11 (MeV)				Probable excited states in ^{22}Ne (MeV)
(a)	(b)	(c)	(d)	
(12.8)	(12.8)			(12.8)
14.47	14.27			14.47
	(15.2)		(16.0)	
	16.45	(16.3)	(16.8)	
(17.8)	(17.7)	17.83	(17.6)	17.8
(18.8)	(18.7)	(18.7)	(18.4)	(18.7)
	(19.9)	20.01	20.0	20.0
(20.8)	(20.8)	(21.3)	20.9	20.9
	(22.2)	(22.2)		
		(23.4)	23.3	23.3
		(24.3)		

gated on the $Q_{gg}(^{10}\text{Be } 3.37/^{18}\text{O} \sim 3.6 \text{ MeV})$ peak is $d^2\sigma/d\Omega_1 d\Omega_2 = (0.054 \pm 0.007) \text{ mb sr}^{-2}$.

Figure 11(d) shows the excitation energy spectrum obtained by gating on the E_{tot} peak corresponding to the $^{14}\text{C}(^{18}\text{O}, ^{22}\text{Ne}^* \rightarrow ^{18}\text{O}^*(\sim 3.6 \text{ MeV}) + \alpha)^{10}\text{Be}^*(3.37 \text{ MeV})$ reaction. As described above the excitation of the ^{10}Be recoil does not affect $E_x(^{22}\text{Ne})$, which has been obtained from $E_{\text{rel}}(^{18}\text{O} + \alpha) - Q_2 + E_x(^{18}\text{O}^*)$. The integrated double-differential cross section for this reaction is $d^2\sigma/d\Omega_1 d\Omega_2 = (0.046 \pm 0.006) \text{ mb sr}^{-2}$.

Columns (a), (b), (c) and (d) in Table II list the centroids of the peaks seen in the corresponding sections of Fig. 11. It is noted that not all of the energies listed in columns (b) and (c) correspond to states. This is due to the uncertainty over the dominant channel populating the $Q_{gg}(^{10}\text{Be } 3.37/^{18}\text{O} \sim 3.6 \text{ MeV})$ peak in Fig. 10. In the final column of Table II the most probable excitation energies for the states in ^{22}Ne that decay to $^{18}\text{O} + \alpha$ are listed. There is no ambiguity in the centroid of the 14.47-MeV peak seen in Fig. 11(a) as the data have been obtained by gating on the clearly identified Q_{ggg} peak in Fig. 10. It is also probable that there are states in ^{22}Ne at approximately 17.8, 18.7, and 20.9 MeV, as there is evidence for peaks close to these energies in all four E_x spectra shown in Fig. 11. A similar argument holds for a state being at $\sim 20.0 \text{ MeV}$ in ^{22}Ne , as peaks are seen at this energy in Figs. 11(b–d). There is some tentative evidence for a state at 12.8 MeV in Fig. 11(a) which would correspond to that seen at this energy in Fig. 11(b), so this energy is also listed in the final column of Table II. Finally, there is also evidence for a state at $\sim 23.3 \text{ MeV}$ in the $^{14}\text{C}(^{18}\text{O}, ^{22}\text{Ne}^* \rightarrow ^{18}\text{O}^*(\sim 3.6 \text{ MeV}) + \alpha)^{10}\text{Be}^*(3.37 \text{ MeV})$ channel seen in Fig. 11(d). It is likely that the only uncertainty in this centroid is the 80-keV difference between the two possible excited states populated by the $^{18}\text{O}^*$ breakup fragment, at 3.55 or 3.63 MeV.

In order to try to distinguish between the energy scales shown in Figs. 11(b) and 11(c), Monte Carlo simulations have been performed for the $^{14}\text{C}(^{18}\text{O}, ^{22}\text{Ne}^* \rightarrow ^{18}\text{O} + \alpha)^{10}\text{Be}$ reaction. The Monte Carlo code [12] simulates the initial excitation of the resonant particle and the sequential decay into two breakup fragments. The resolution contributions to the reconstructed E_{tot} and E_x spectra due to a number of effects, including beam spot size, energy spread, divergence and energy loss in the target, fragment energy and angular straggle and energy loss in the target, and detector energy and position resolutions, may be studied. The $Q_{ggg}(^{14}\text{C})$ peak seen in Fig. 1 has a measured width of $(1227 \pm 40) \text{ keV}$ that compares well to the simulated width of $(1248 \pm 45) \text{ keV}$. This value is dominated by the energy spread in the beam following acceleration by the LINAC. The state at $E_x = 8.04 \text{ MeV}$ in Fig. 4 has a natural width of $< 2.5 \text{ keV}$ [13]. This indicates that the measured width, $(94 \pm 1) \text{ keV}$, is dominated by the experimental excitation energy resolution. This is predicted to be $(88 \pm 3) \text{ keV}$ by the Monte Carlo code, the major contribution to this width being due to the detector position resolution. This good agreement between the experimentally measured and the predicted widths indicates that the input parameters used in the

simulations are valid. The same parameters were also used to study the $^{14}\text{C}(^{18}\text{O}, ^{22}\text{Ne}^* \rightarrow ^{18}\text{O}_{\text{g.s.}} + \alpha)^{10}\text{Be}_{\text{g.s.}}$ reaction. The width of the Q_{ggg} peak seen in Fig. 10 is $(1151 \pm 124) \text{ keV}$ which again compares favorably with the predicted value of $(1173 \pm 40) \text{ keV}$. The simulated excitation energy resolution for the 14.47-MeV state shown in Fig. 11(a) is $(235 \pm 9) \text{ keV}$. This suggests that the observed width of $(400 \pm 50) \text{ keV}$ is either due to a number of overlapping unresolved states or that a broad natural width is observed. Subtracting the predicted resolution from the measured value in quadrature indicates a natural width of $(324 \pm 46) \text{ keV}$, assuming that the peak is comprised of a single state.

The predicted width, $(281 \pm 12) \text{ keV}$, for the 20.01 MeV state seen in Fig. 11(c) is again less than the experimentally observed value of $(420 \pm 74) \text{ keV}$, indicating that the peak may be a doublet. This simulated width reduces to $(259 \pm 10) \text{ keV}$ if the energy scale in Fig. 11(b) is assumed to be correct, placing the peak at 16.45 MeV. This slight decrease in value is a general feature of sequential binary breakup, with experimental E_x resolution improving as the excitation energy reduces towards the reaction threshold. The effect of the in-flight γ decay of the 3.37-MeV first-excited state of ^{10}Be in the $^{14}\text{C}(^{18}\text{O}, ^{22}\text{Ne}^* \rightarrow ^{18}\text{O}_{\text{g.s.}} + \alpha)^{10}\text{Be}^*(3.37 \text{ MeV})$ reaction assumed in Fig. 11(b) is to increase the predicted width of the 16.45-MeV state to $(272 \pm 11) \text{ keV}$. Therefore the Monte Carlo simulated widths of 280 and 270 keV for the 420-keV-wide peak seen in Figs. 11(b) and 11(c) at 20.01 and 16.45 MeV, respectively, cannot distinguish between the two possible energy scales.

Because the recoiling ^{10}Be has been detected in the events shown in Fig. 11 and the kinematics of the ^{18}O reconstructed, the θ^*/ψ angular correlation coverage is very limited for this channel. For this reason no spin information is available for the observed states.

IV. SUMMARY AND CONCLUSIONS

The $^{14}\text{C}(^{18}\text{O}, ^{14}\text{C } \alpha)^{14}\text{C}$ reaction has been studied at 102 MeV. The coincident detection of the ^{14}C and α breakup fragments from the decay of excited states in ^{18}O has allowed the spins of the decaying states to be studied. The data provide evidence that a molecular rotational band, identified by the enhanced α decay of the band members, is populated in the reaction. The measured rotational parameter indicates that the structure has a large moment of inertia and is consistent with a quasimolecular configuration. Evidence is also provided for the $^{18}\text{O} + \alpha$ breakup of ^{22}Ne from a number of states at a high excitation energy, in the range 12–24 MeV.

ACKNOWLEDGMENTS

The authors would like to thank Powell Barber for his assistance in preparing the ^{14}C target. This work was supported in part by the National Science Foundation under Grant No. 9970991.

- [1] Y. Alhassid, M. Gai, and G. F. Bertsch, *Phys. Rev. Lett.* **49**, 1482 (1982).
- [2] M. Gai, M. Ruscev, A. C. Hayes, J. F. Ennis, R. Keddy, E. C. Schloemer, S. M. Sterbenz, and D. A. Bromley, *Phys. Rev. Lett.* **50**, 239 (1983).
- [3] P. Descouvemont and D. Baye, *Phys. Rev. C* **31**, 2274 (1985).
- [4] Y. Suzuki, A. Yamamoto, and K. Ikeda, *Nucl. Phys.* **A444**, 365 (1985).
- [5] M. Gai, R. Keddy, D. A. Bromley, J. W. Olness, and E. K. Warburton, *Phys. Rev. C* **36**, 1256 (1987).
- [6] M. Gai, M. Ruscev, D. A. Bromley, and J. W. Olness, *Phys. Rev. C* **43**, 2127 (1991).
- [7] G. Reidemeister and F. Michel, *Phys. Rev. C* **47**, R1846 (1993).
- [8] W. D. M. Rae and R. K. Bhowmik, *Nucl. Phys.* **A420**, 320 (1984); **A427**, 142 (1984); R. K. Bhowmik, W. D. M. Rae, and B. R. Fulton, *Phys. Lett.* **136B**, 149 (1984).
- [9] N. Curtis, A. St. J. Murphy, M. J. Leddy, J. S. Pople, N. M. Clarke, M. Freer, B. R. Fulton, S. J. Hall, G. Tungate, R. P. Ward, S. M. Singer, W. N. Catford, G. J. Gyapong, R. A. Cunningham, J. S. Lilley, S. P. G. Chappell, S. P. Fox, C. D. Jones, D. L. Watson, P. M. Simmons, R. A. Hunt, A. C. Merchant, A. E. Smith, W. D. M. Rae, and J. Zhang, *Nucl. Instrum. Methods Phys. Res. A* **351**, 359 (1994).
- [10] S. Marsh and W. D. M. Rae, *Phys. Lett.* **153B**, 21 (1985).
- [11] M. Freer, *Nucl. Instrum. Methods Phys. Res. A* **383**, 463 (1996).
- [12] N. Curtis, N. M. Clarke, B. R. Fulton, S. J. Hall, M. J. Leddy, A. St. J. Murphy, J. S. Pople, R. P. Ward, W. N. Catford, G. J. Gyapong, S. M. Singer, S. P. G. Chappell, S. P. Fox, C. D. Jones, D. L. Watson, W. D. M. Rae, and P. M. Simmons, *Phys. Rev. C* **51**, 1554 (1995).
- [13] D. R. Tilley, H. R. Weller, C. M. Cheves, and R. M. Chasteler, *Nucl. Phys.* **A595**, 1 (1995).
- [14] B. R. Fulton, S. J. Bennett, M. Freer, J. T. Murgatroyd, G. J. Gyapong, N. S. Jarvis, C. D. Jones, D. L. Watson, J. D. Brown, W. D. M. Rae, A. E. Smith, and J. S. Lilley, *Phys. Lett.* **267**, 325 (1991).
- [15] P. A. Butler and W. Nazarewicz, *Rev. Mod. Phys.* **68**, 349 (1996).
- [16] F. Ajzenberg-Selove, *Nucl. Phys.* **A475**, 1 (1987).